Geometrically Calibrated Network Models for Progressive Cavity Pump Design

Geometrically Calibrated Network Models for Progressive Cavity Pump Design

Kevin Simon and **Alexander H. Slocum**, Massachusetts Institute of Technology

Abstract

Linear network models are promisingly simple Progressive Cavity Pump design tools. Current linear network models are difficult to use in the design process because they require calibration against experimental data or computationally intensive simulation. This paper presents new approaches for implementing linear network Progressive Cavity Pump models, and provides new methods to accurately and quickly estimate the values of each resistor in the model from pump geometry for both laminar and turbulent flows. This paper also argues that sealing-line flow transitions from laminar to turbulent at orders of magnitude smaller Reynolds Number than described in literature thus far. It proposes a new hypothesis for the point of transition to turbulent performance.

1.0. Introduction

Progressive Cavity Pumps (PCPs) are rotary positive displacements pumps with exceptional properties. They have the high-performance of positive displacement pumps; require no specialized seals; deliver near-pulsation-free flow; and have only one moving part. In the most common configuration, PCPs consist of a single-helix rotor eccentrically orbiting inside a double-helix, driving the working fluid axially through the pump in a spiral, **Fig. 1**. In spite of these advantages, PCPs are limited in use to high-end applications such as deep-well lift and chemical processing. High manufacturing costs and analytical complexity are among the main reasons for limited PCP adoption.

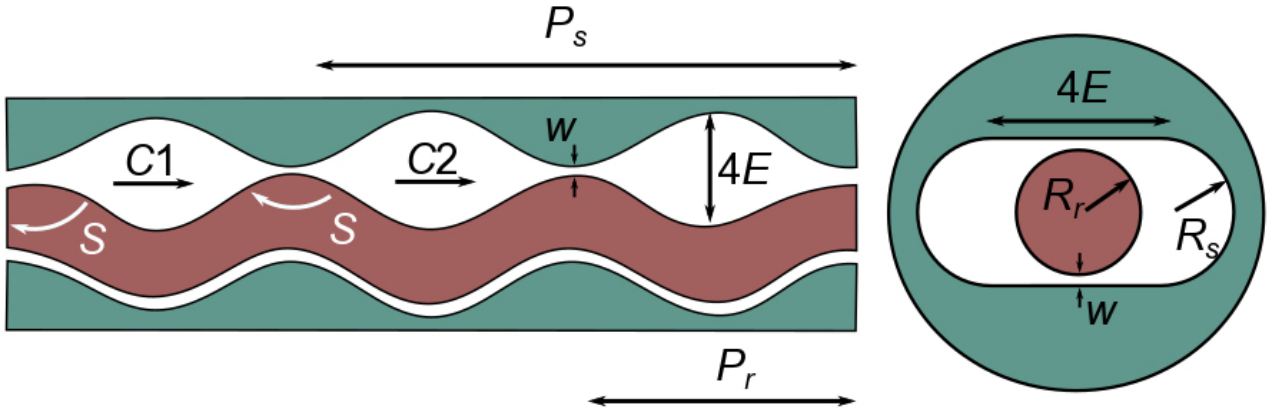

Fig. 1—A depiction of typical PCP geometry from the side (left) and in cross-section (right). C1 and C2 represent separate cavities. P_s = nominal stator pitch; P_r = nominal rotor pitch; R_s = nominal stator radius; R_r = nominal rotor radius; S = slip flow rate; w = nominal clearance gap; E = rotor eccentricity.

There are four categories of PCP models: first-order models based on Poieuselle-Couette flow (Moineau 1930; Vetter and Wirth 1995); cavity network models (Gamboa et al. 2002; Pessoa et al. 2009); lubrication theory models (Andrade et al. 2011); and a variety of full computational fluid dynamics (CFD) models (Chen et al. 2013; Paladino et al. 2009; Berton et al. 2011; Zhou et al. 2013). Even though there is a wide range of tools for predicting the performance of PCPs, there is a gap in modeling turbulence easily enough to enable rapid exploration of the design space to optimize a new PCP. Current network models require

Original SPE manuscript received for review XX YY 20ZZ. Revised manuscript received for review XX YY 20ZZ. Paper (SPE XX) peer approved XX YY 20ZZ.

calibration against CFD or experimental tests, and the state-of-the-art lubrication theory model is unable to handle turbulent flows. First-order models lack the predictive capability to design PCPs. CFD of PCPs is time-intensive, and requires significant expertise.

To develop new PCPs for use with low-viscosity fluids, such as water, this paper presents newly adapted methods for estimating the performance of a PCP with turbulent flows. These methods are important because low-viscosity fluids are prevalent in artificial lift systems. Water and high-temperature hydrocarbons from oil sands extraction are two noteworthy examples. Without reduced-order models for turbulent operation, the design engineer's analytical toolbox is limited. Additionally, this work presents new ways of constructing and calibrating models for laminar flow.

The method presented directly and efficiently calculates the critical geometric parameters for a network model and lends itself to efficient pairing with lubrication-theory analysis of PCPs. The model is then compared with experimental data from literature to confirm its accuracy over a range of geometries, in both laminar and turbulent conditions.

The linear network model presented by Pessoa et al. (2009) has shown promise for understanding the performance of pumps that have already been modeled or extensively tested. Due to the extent of manual calibration that it requires, their methods have limited applicability to the early stage of pump conceptualization, i.e. when choosing between pump types. This section includes a refinement of their method, and a process for integrating the lubrication theory model into the linear network calibration process to rapidly get a physical understanding of PCP mechanics.

2.0. Network Models

2.1. Background PCPs can be modeled as devices that deliver fluid at a known rate, Q_{th}, minus a slip flow, S, as expressed in Eq. 2. Because Q_{th} is straightforward to compute, see Eqs. 1 (Belcher 1991), the challenge of this approach is in modeling the slip flow. The simplest way to model the slip flow is with a fluidic resistor analog, shown in **Fig. 2**. One way to model the resistance of a fluid element is with the Darcy-Weisbach equation, which assumes that the pressure difference across a channel is proportional to the dynamic pressure of the fluid and the channel aspect ratio (hydraulic diameter to length) Eq. 3. Here, U is the area averaged fluid velocity, l_s is the channel length, and D_h is the hydraulic diameter. The Darcy friction factor, f, is that coefficient of proportionality. The term $f_{laminar}$ is the laminar correlation for f in Pessoa's model (2009), and is calculated with Eq. 4.

$$Q_{th} = \frac{4}{\pi} E R_r P_s \Omega \tag{1}$$

$$Q = Q_{th} - S \tag{2}$$

Fluid network models for PCPs assume that each cavity has uniform pressure. These network models are robust, fast, and easy to understand. Most require calibration to experimental data or numerical simulation, although Zheng et al. (2018) have recently developed a promising technique for estimating laminar flow resistance directly from geometry. This section discusses different strategies that can estimate the resistance of the sealing lines.

$$\Delta P = f \frac{l_s}{D_h} \frac{\rho U^2}{2} \tag{3}$$

$$f_{laminar} = \frac{64}{\mathrm{Re}} \tag{4}$$

$$S = U w b \tag{5}$$

$$D_h = 2w \tag{6}$$

$$\mathrm{Re} = \frac{U D_h}{\nu} = \frac{2S}{\nu b} \tag{7}$$

$$\Delta P = C_p \frac{\rho U^2}{2} \tag{8}$$

Pessoa et al. (2009), whose work this is largely based upon, uses the friction factor correlation for straight ducts, Eq. 3, to estimate the flow resistance of PCP sealing lines. Since l_s is used as a calibration factor in their work, it can obscure the nature of the model. Furthermore, the equivalent pipe resistor model requires non-physically large surface roughness to hydraulic diameter ratios, on the order of 0.1, to match experimental data. An alternative pressure loss modeling approach assumes that the pressure drop is proportional to the dynamic pressure of the jet exiting the resistor, represented in Eq. 8 (Edwards et al. 1985). There are two advantages to this formulation. It is more transparent about the nature of the assumptions, and it enables for a more nuanced discussion of the flow resistance mechanisms.

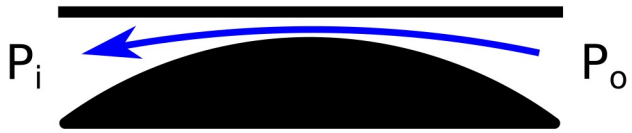

Fig. 2—A depiction of a single flow resistor.

$$C_{pL} = \frac{K}{\mathrm{Re}} \tag{9}$$

$$\Delta P_L = S\frac{\mu K}{2bw^2} \tag{10}$$

$$b_{long} = \pi R_s \tag{11}$$

$$\frac{\partial X_r}{\partial \Theta_s} = -2E\cos(2\Theta_s) \tag{12}$$

$$\frac{\partial Y_r}{\partial \Theta_s} = -2E\sin(2\Theta_s) \tag{13}$$

$$\frac{\partial Z_r}{\partial \Theta_s} = \frac{P_s}{2\pi} \tag{14}$$

$$b_{trans} = \int_0^{\pi} \sqrt{\left(\frac{\partial X_r}{\partial \Theta_s}\right)^2 + \left(\frac{\partial Y_r}{\partial \Theta_s}\right)^2 + \left(\frac{\partial Z_r}{\partial \Theta_s}\right)^2}\, d\Theta_s \tag{15}$$

Most fluid fittings and connections are modeled by a static pressure loss coefficient, C_p, which is inversely proportional to Re in the laminar regime, C_{pL}, and constant with respect to Re in the turbulent regime, C_{pT}. Equation 8 is consistent with that convention, and enables better articulated comparisons between the flow characteristics in PCP sealing lines and other flow restricting devices. The pipe analogy used to formulate Eq. 3 for PCP seal line modeling introduces an extra hydraulic diameter, D_h, term along with the l_s calibration term. Given that the static pressure loss coefficient formulation is more commonly used to model flows in complex geometries, the authors encourage the use of Eq. 8 over Eq. 3 (Edwards et al. 1985; Fester et al. 2007; Greitzer et al. 2004). As such, the rest of the network modeling work discussed here will also center around Eq. 8.

Equations 8 and 7 connect the sealing line geometry to the laminar flow resistance, Eq. 10. A detailed description of how to compute the longitudinal and transverse sealing line widths, b_{long} and b_{trans} respectively, is in Pessoa's original paper (Pessoa et al. 2009). w is the sealing line height, μ is the dynamic viscosity, and U is the average fluid velocity in the channel. For many static flow components, the pressure drop coefficient is independent of Re in the turbulent regime (Edwards et al. 1985). While this is a large assumption, it provides remarkably good predictions and is an excellent starting point for discussing the role of turbulence in the mechanics of PCP flow. This results in Eq. 16 as an estimate for nonlinear turbulent flow resistance between cavities.

$$\Delta P_T = S^2\frac{C_{pT}\rho}{2b^2w^2} \tag{16}$$

$$C_{pT} \approx \left(1 - \frac{1}{\mathrm{AR}}\right)^2 \tag{17}$$

Equation 17 is a commonly accepted estimate for the pressure loss coefficient of a mixing jet (Greitzer et al. 2004). In this case, AR is the area ratio between the vena contracta of the orifice jet and the surrounding cavity. For a PCP, AR is approximately $w/(4E)$. Because $w << 4E$, C_{pT} is close to 1. This assumption should be revisited if a PCP with large clearances or small cavities is ever designed. For the orifice model, it is assumed that the flow separates immediately downstream of the narrowest point. This assumption implies that the seals act as perfectly imperfect diffusers where none of the kinetic energy in the dynamic pressure created by acceleration through the seal is recovered.

The results from Edwards' work (1985) can also be used to estimate when flow through the sealing line transitions from laminar to turbulent. In Edwards' experiments, the flows in the fittings transition to turbulent when the laminar coefficient of friction becomes approximately equal to the turbulent coefficient of friction. This conclusion was also put forward by Fester et al. (2007). For the progressive cavity pump sealing lines examined in this paper, and likely others as well, C_{pT} is approximately 1. Therefore, it is hypothesized that the transition to turbulence in PCP seals likely occurs when $\mathrm{Re} \approx K$, Eq. 9. While this might seem obvious to some readers, it is very different from pipe flow, where $K = 64$, but the transition to turbulence occurs at

approximately Re=1,500, where C_{pT} transitions to its turbulent value. This is a useful design hypothesis, because it enables for pump designers to begin to predict what slip flow magnitude will induce turbulent flow for a given pump geometry. Additionally, it often predicts the transition an order of magnitude earlier than most PCP research papers in the current literature.

2.2. Extension of Network Model Before discussing new deterministic calibration procedures for the sealing line resistances, K, the structure of the fluid network model needs to be refined. This section presents clarifications and modifications on Pessoa's original model (2009). The general structure of a single lobe PCP resistor network is depicted in **Fig. 3**. Since Pessoa's model (2009) is already calibrated by a single coefficient, sealing length: l_s, it may seem unnecessary to focus in detail on terms which may simply be calibrated out. However, it will be demonstrated that small changes in the model structure has a significant impact on the predictive capabilities of the tool, and the intuition for PCP performance that it builds.

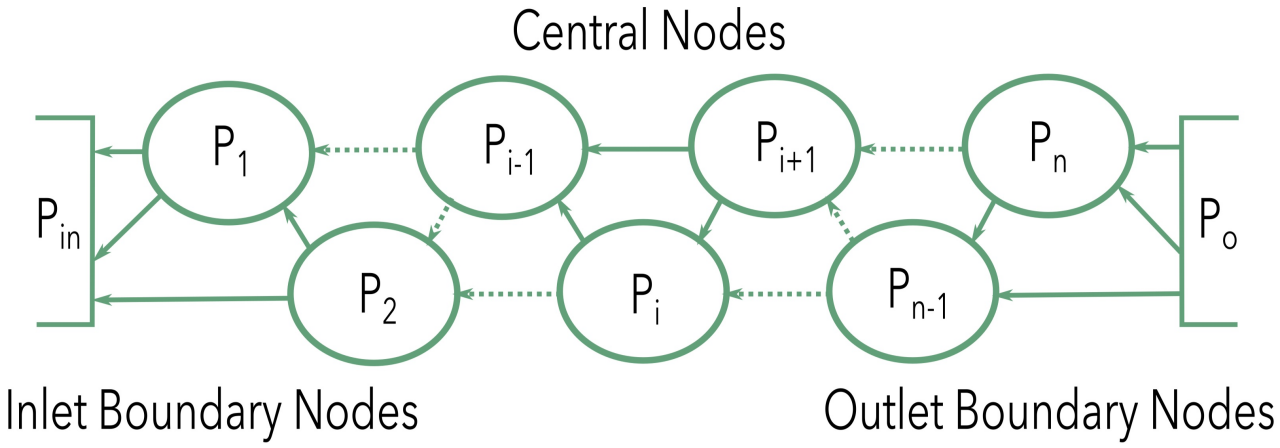

Fig. 3—Illustration of the cavity nodes and connectivity in a PCP network model. The arrows represent slip flow between cavities.

2.2.1. Boundary Conditions and the Right Hand Side Pessoa et al. (2009) previously presented a powerful application of linear networks to modeling PCP performance. A few elements of their work were unclear to the authors. As such, this section begins with specific definitions for those elements as a starting block for this work. Pessoa's paper does not include a specific formulation for the right hand side of the resistor network system of equations. It is inferred, based on Eq. 18 for slip flow from Pessoa's paper, that the pump outlet is connected to the last node by one transverse sealing line, and to the second-to-last node by one longitudinal sealing line.

$$S = \frac{\Delta P_{n\to n-2}}{R_L} + \frac{\Delta P_{n\to n-1}}{R_T} \tag{18}$$

The new slip flow formulation proposed in this work, Eq. 19, assumes that both longitudinal and transverse slip flow occurs between the pump outlet and the final cavity. This assumption is reasonable given the general geometry of PCPs shown in **Fig. 4**, generated using lubrication theory (Andrade et al. 2011). Further inspection of equivalent ghost nodes for the network outlet also reveals that there are indeed three leakage paths to the outlet. Equation 20 is the equation for the network with boundary conditions. $T = 1/R_T$, $L = 1/R_L$, and $A = 2(L+T)$.

$$S = \frac{\Delta P_{o\to n}}{R_T} + \frac{\Delta P_{o\to n}}{R_L} + \frac{\Delta P_{o\to n-1}}{R_L} \tag{19}$$

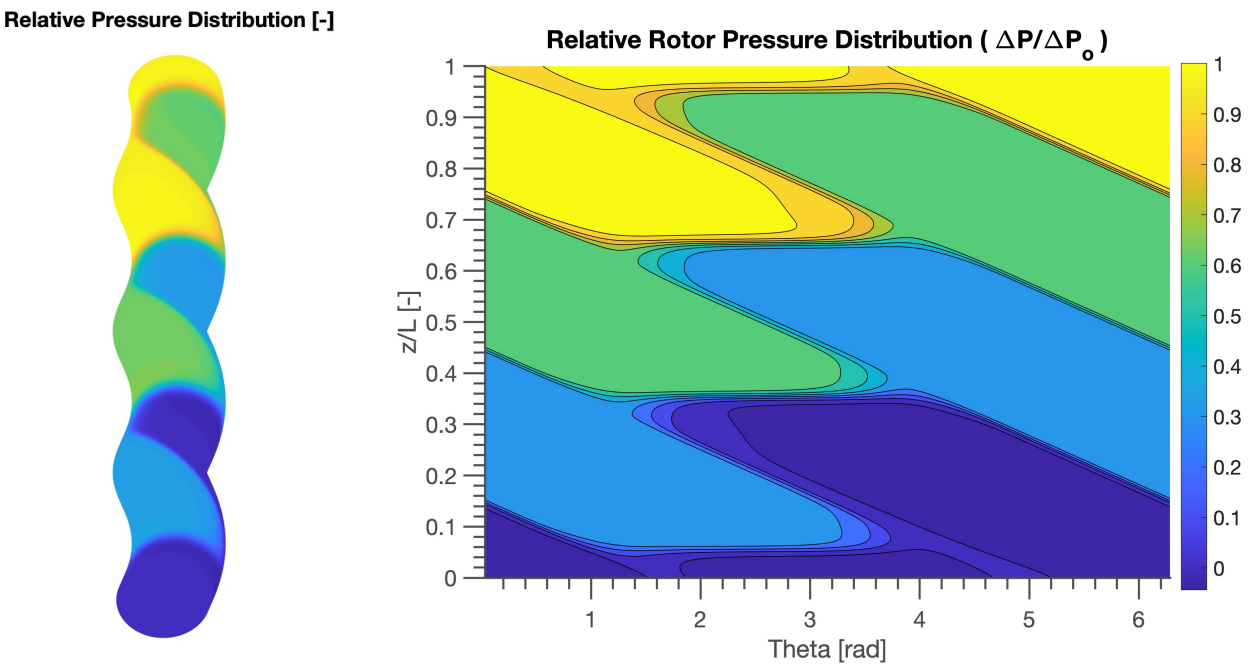

Fig. 4—Pressure distribution along the rotor of a representative two cavity pump. Transverse sealing lines connect cavities that are two nodes apart, and are horizontal lines. Longitudinal sealing lines connect neighboring cavities, and appear at an angle.

$$\begin{bmatrix} \ddots & \ddots & \ddots & \ddots & \ddots & \ddots & \ddots \\ \ddots & -A_{i-2} & T_{i-1} & L_i & 0 & 0 & \ddots \\ \ddots & T_{i-2} & -A_{i-1} & T_i & L_{i+1} & 0 & \ddots \\ \ddots & L_{i-2} & T_{i-1} & -A_i & T_{i+1} & L_{i+2} & \ddots \\ \ddots & 0 & L_{i-1} & T_i & -A_{i+1} & T_{i+2} & \ddots \\ \ddots & 0 & 0 & L_i & T_{i+1} & -A_{i+2} & \ddots \\ \ddots & \ddots & \ddots & \ddots & \ddots & \ddots & \ddots \end{bmatrix} \begin{bmatrix} \vdots \\ P_{i-2} \\ P_{i-1} \\ P_i \\ P_{i+1} \\ P_{i+2} \\ \vdots \end{bmatrix} = \begin{bmatrix} 0 \\ \vdots \\ 0 \\ 0 \\ 0 \\ 0 \\ 0 \\ \vdots \\ P_o L_{n-1} \\ P_o(T_n + L_n) \end{bmatrix} \tag{20}$$

2.2.2. Differences in Pressure Drop Coefficients Given the differences in rotor and stator curvature on the longitudinal and transverse sealing lines, it is assumed that T and L have different values, respectively. All values for T are assumed to be identical, and the same assumption applies to all values of L. For the reader who is skeptical of this delineation, a simple proof of the importance of treating the two sealing line types differently is presented below. A two cavity pump can be represented by the mass balance for a linear network with Eq 21, where $T = 1/R_T$ and $L = 1/R_L$.

$$\begin{bmatrix} L & T & -A & T & L & 0 \\ 0 & L & T & -A & T & L \end{bmatrix} \begin{bmatrix} 0 \\ 0 \\ P_1 \\ P_2 \\ P_o \\ P_o \end{bmatrix} = \begin{bmatrix} 0 \\ 0 \end{bmatrix} \tag{21}$$

After normalizing the equation such that $T^* = T/A$ and $L^* = L/A$, Eq. 21 simplifies to Eq. 22.

$$\begin{bmatrix} 1 & -T^* \\ -T^* & 1 \end{bmatrix} \begin{bmatrix} P_1 \\ P_2 \end{bmatrix} = P_o \begin{bmatrix} L^* \\ 0.5 \end{bmatrix} \tag{22}$$

The solution is:

$$P_1 = P_o \left[L^* + T^* \left(\frac{L^* T^* + 0.5}{1 - T^{*2}} \right) \right] \tag{23}$$

$$P_2 = P_o \left(\frac{L^* T^* + 0.5}{1 - T^{*2}} \right) \tag{24}$$

In the simplest of cases, when $L^* = T^* = 0.25$, $P_1 = 0.4P_o$ and $P_2 = 0.6P_o$. This result indicates that the ratio of the sealing values plays an important role in determining the pressures in each cavity. The results from the lubrication theory model, shown in Fig. 4, predict that $P_1 = 0.34P_o$ and $P_2 = 0.65P_o$. This matches qualitative descriptions of linear cavity pressure distributions in literature, and indicates that longitudinal sealing lines are the driving leak path connecting neighboring cavities.

2.2.3. Calibration Algorithm The network formulation presented here can quickly determine L and T with one result from the lubrication theory model presented developed by Andrade et al. (2011), which is a first-principles model that has shown strong agreement with experimental data. The calculation begins with results from a lubrication theory simulation of a two cavity PCP with in a fluid where Re < 50 and all other geometric variables taken from the pump design: R_r, R_s, P_s, P_r, E, w. The matrix $\mathbf{A}$ in Eq. 26 is constructed from the simulation results, S, P_1, P_2, and P_o. $\mathbf{A}$ is then input to Eq. 27. The first two rows of $\mathbf{A}$ come from Eq. 21, and the bottom row is based on Eq. 19, the equation for the outlet slip flow, S. Equations 25 and 26 represent the same system of equations.

$$\begin{bmatrix} -2(L+T) & T & L \\ T & -2(L+T) & T+L \\ -L & -(L+T) & 2L+T \end{bmatrix} \begin{bmatrix} P_1 \\ P_2 \\ P_o \end{bmatrix} = \begin{bmatrix} 0 \\ 0 \\ S \end{bmatrix} \tag{25}$$

$$\begin{bmatrix} P_2 - 2P_1 & P_o - 2P_1 \\ P_1 - 2P_2 + P_o & P_o - 2P_2 \\ P_o - P_2 & 2P_o - P_1 - P_2 \end{bmatrix} \begin{bmatrix} T \\ L \end{bmatrix} = \mathbf{A} \begin{bmatrix} T \\ L \end{bmatrix} = \begin{bmatrix} 0 \\ 0 \\ S \end{bmatrix} \tag{26}$$

Since the 3x2 matrix, $(\mathbf{A})$, in Eq. 26 is not square, the Moore-Penrose inverse computes L and T in Eq. 27.

$$\begin{bmatrix} T \\ L \end{bmatrix} = (\mathbf{A^T A})^{-1} \mathbf{A^T} \begin{bmatrix} 0 \\ 0 \\ S \end{bmatrix} \tag{27}$$

After computing the total resistance for the transverse and longitudinal sealing lines, the known geometric parameters specify the laminar viscous coefficient, K, with Eqs. 28 and 29.

$$K_T = \frac{2 b_{trans} w^2}{T \mu} \tag{28}$$

$$K_L = \frac{2 b_{long} w^2}{L \mu} \tag{29}$$

The two pressure loss coefficient, single sealing length, and the single sealing length with old boundary conditions (see above) were all calibrated against a two cavity PCP using Eq. 27 and then used to predict the performance of a four cavity PCP with the other geometric parameters held constant. Table 1 shows the distribution of pressures inside of a four cavity PCP. In accordance with the methods described by Pessoa et al. (2009), the single sealing length models were calibrated manually, iterating until the model matched the data. The two pressure loss coefficient model was calibrated with Eq. 27.

The two pressure loss coefficient model shows better agreement with the lubrication theory model than either of the single sealing line length models. The first and last cavities of the single sealing length model are off by 5% of the outlet pressure, while the single sealing length model with simple boundary conditions has a non-physical pressure distribution, see the last column of Table 1.

The data from Gamboa et al. (2003) were also included for the four cavity PCP for reference. The specific Gamboa data are for 0% gas volume fraction operation with 0.042 Pa-s oil running at 400 rpm. The pressure measurements are from just before the pressure spikes at 180°. P_o for the Gamboa data was specified assuming that there is a 826.13 kPa pressure differential across the pump. These data match the two sealing length and lubrication theory model to within 2%.

Value	Gamboa	Lubrication	2 Seals	1 Sealing Length	Simple BC
P_1/P_o	0.210	0.211	0.211	0.251	0.187
P_2/P_o	0.398	0.405	0.403	0.400	0.277
P_3/P_o	0.595	0.600	0.597	0.600	0.4749
P_4/P_o	0.812	0.792	0.788	0.750	0.443

Table 1—The pressure profiles of different PCP models for the 4 sealing cavity PCP. The linear models were calibrated against a two cavity PCP lubrication simulation, and were simulated with Re $\approx$ 50.

2.2.4. Independence of K_L and K_T This section presents the sensitivity of K to different PCP design variables. With the new orifice network formulation herein, it is possible to separate sealing line length, K_L and K_T, from the number of cavities. It is valuable to know what factors drive the pressure loss coefficient, and what factors are independent of K. The design variables that could affect the viscous pressure loss coefficient are listed below. Some of these design variables have a direct influence on sealing line performance, but they all have additional nonlinear influence through cross coupling with K. It has been shown in Table 1 that K is independent of the number of pitches. **Figure 5** is an example of how K varies with geometric variables. In this case, the base design is the pump from the work by Gamboa et al. (2002). Note that varying multiple geometric variables at the same time may result in nonlinear cross terms not portrayed in Fig. 5.

- w: The clearance gap appears separately from K in the flow resistance equations, PCP performance is very sensitive to w, it makes sense that w and K have a co-dependence.
- P_r: The rotor pitch, and, by kinematics, the stator pitch directly affects the curvature of the sealing line, so K is dependent on it.
- E: The pump eccentricity should mostly affect sealing line width, and have a minimal impact on K.
- R_r: The rotor radius directly affects the curvature of the sealing lines, so it plays a role in determining K.

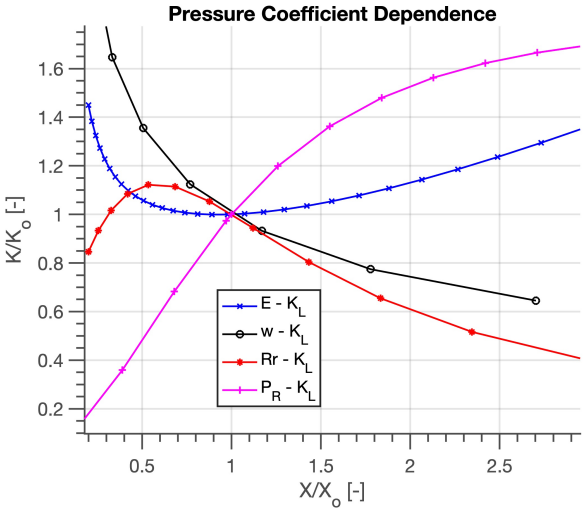

Fig. 5—The effect of different geometric variables on the longitudinal pressure loss coefficient. Higher values of K/K_o indicate better geometry-independent sealing and delayed transition to turbulence.

2.3. Model Validation The orifice network model shows agreement with experimental data from literature. **Figure 6** shows both the turbulent data from Gamboa et al. (2003) and Vetter and Wirth (1995) alongside the model's predictions. The orifice network model has similar agreement with the data as the equivalent pipe resistor model by Pessoa et al. (2009). This makes sense because both functions have the same quadratic pressure and flow relationship. Gamboa's experimental results have been extensively studied, and other linear networks have shown the same degree of agreement after manual calibration. The Reynolds numbers for flow inside the seals of the water Gamboa experiment range from 1,000 to 9,000. The pump used in Vetter's experiments has not been tested at low Reynolds numbers, making manual calibration of a network model unfeasible.

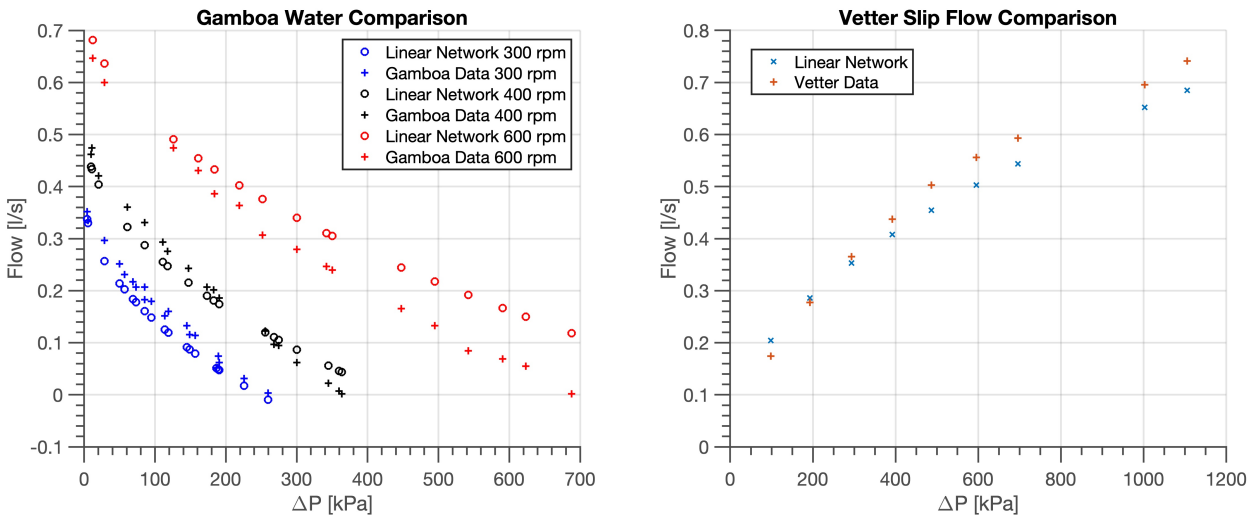

Fig. 6—Results from the orifice network model compared with experimental data from Gamboa et al. (2002), Vetter and Wirth (1995).

The orifice network model was able to accurately and quickly capture their performance results without any calibration beyond setting C_{pT} to 1.

Given these differences, it is likely that there are flow mechanisms which are not accounted for by Eqs. 8 and 16. Idelchik and Fried (1986) have noted that diverging curved channels have a greater turbulent and friction resistances than equivalent straight channels. Pessoa et al. (2009) also noted that 'one of the strongest hypotheses in these approaches is the simplification of the channel geometry'. While experimental comparison shows the orifice network's impressive ability to model flow performance, the turbulent pressure loss correlation still leaves room for improvement in the model.

Since this model is capable of efficiently estimating turbulent flow through PCP channels, the orifice network model could be coupled with a deformation model for a compliant stator or rotor.

2.4. Combined Turbulent and Lubrication Flow Resistance If the earlier hypothesis that turbulent jet mixing downstream of the resistor is the primary mechanism for turbulent flow resistance, then it stands to reason that the viscous momentum transfer mechanisms, such as the ones observed in the laminar resistor model, are still present in the flow. Therefore a combined turbulent and laminar resistor, resembling a long orifice shown in **Fig. 7**, as described in Eq. 30 can provide more predictive power. The term is inspired by Miller (1978).

$$\Delta P_{TL} = S^2 \frac{C_{pT}\rho}{2b^2w^2} + S\frac{\mu K}{2bw^2} \tag{30}$$

K was computed using the laminar methodology described in Extension of the Network Model. With the addition of a new flow resistance mechanism, C_{pT} needed to be reduced to 0.8 to match the data from Gamboa and Vetter. A C_{pT} value of slightly less than one implies a small degree of pressure recovery. This indicates that flow separation occurs a small distance downstream of the flow expansion.

As **Fig. 8** shows, the empirical loss coefficient of 0.8 and the geometrically driven K value show excellent agreement with experimental data for two different pumps operated across a wide range of speeds, pressure, and length-scales. It must be admitted that the addition of complexity to a model can increase predictive power without necessarily using better physics.

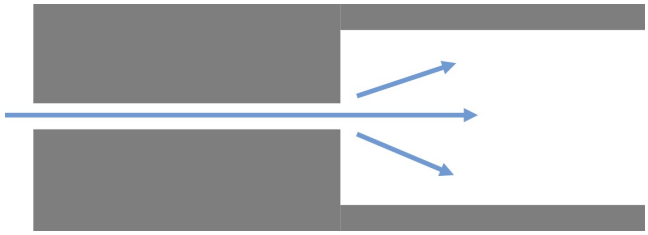

Fig. 7—A long orifice, made of a viscous channel followed by a mixing dominated sudden expansion.

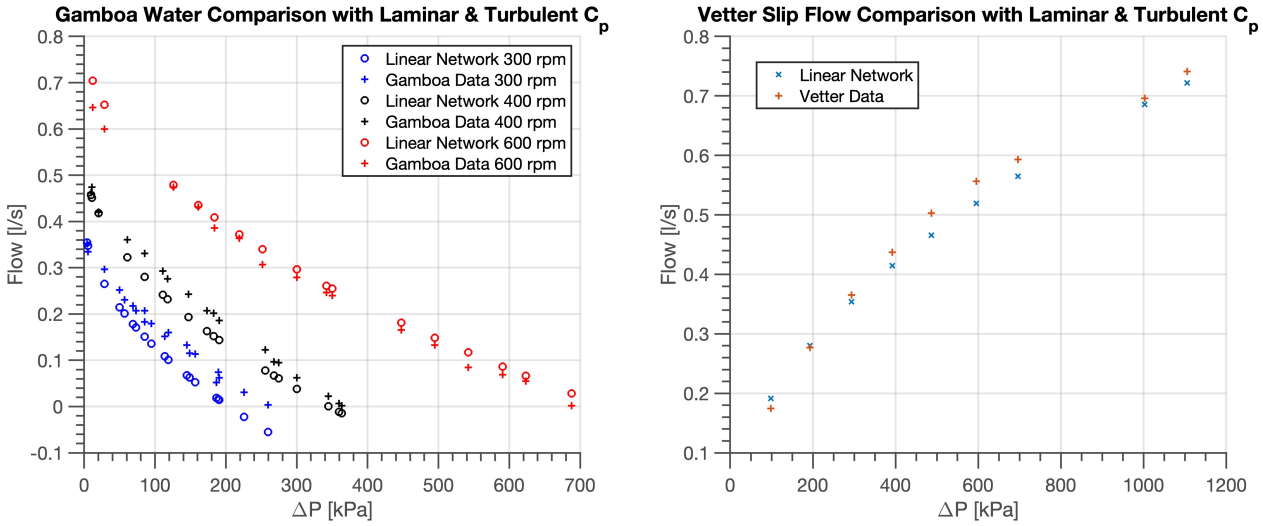

Fig. 8—Results from the long orifice network model compared with experimental data from Gamboa et al. (2002), Vetter and Wirth (1995).

Fortunately, the structure of this model makes physical sense: it is possible for momentum to be dissipated by both viscosity in a channel and jet mixing downstream of the channel. This is different from the previous laminar/turbulent equivalent pipe friction factor. In that formulation, it would not make sense to combine viscous and turbulent resistances in series. Since K is computed from first principles using lubrication theory, only one term, C_{pT}, is necessary to fit the model. A C_{pT} of 0.8 is physically plausible, especially when compared to the surface roughness to diameter ratio, ε/D, of approximately 0.1 is necessary to fit the equivalent turbulent pipe model to data.

As such, the authors recommend this long orifice network model as the turbulent model for PCP design. It provides remarkable turbulent predictive capability; a prediction for the transition to turbulence; and has a minimal increased computational cost compared to the $C_{pT} = 1$ model because of the efficiency of the lubrication theory model.

3.0. Conclusion

The goal of this work was to create a computationally efficient model for turbulent flow within a PCP, using only pump geometry and fluid properties as inputs. This work presents improvements over existing work in literature by combining the strengths of both PCP lubrication theory and network modeling. The lubrication model can define geometric parameters necessary for the network model without needing experimental data or full CFD to perform manual calibration. The network model uses the effective sealing length to model turbulent operation. The accuracy of this method has been tested against experimental data produced by Gamboa and Vetter across a wide range of Reynolds numbers.

The model presented in this paper has the ability to simplify and accelerate the PCP design process for applications with turbulent flow. Notably, these models also provide a new way to estimate if the sealing lines are under laminar or turbulent conditions.

These models are not formulated for more than two different sealing line types. Methods for calibrating against more than two sealing line types will be essential for extending this work to deformable stator/rotor pumps; compressor-type pumps with varying cavity size; or pumps with significantly varying seal geometry due to manufacturing tolerances. This would enable pump designers to deterministically set tolerances for the complex rotor and stator geometries. Although a new method for predicting the transition from laminar sealing line flow to turbulent sealing line flow has been presented, the fluid behavior in that transition is still poorly understood. Additionally, this model is not applicable to multi-lobe PCPs. Each of these limitations are opportunities for future research.

This work has implications beyond the design of PCPs. This strategy for using discrete and continuum models together to attain improved accuracy can be applied to other problems with complex and multi-length-scale mechanics. Furthermore, this method can likely be applied to the design of other types of positive displacement pumps.

4.0. Acknowledgements

The authors would like to thank the Tata Center for Technology and Design at MIT for sponsoring this work.

Authors

Kevin Simon is a research engineer at Watts Water Technologies Inc. He holds a BS in mechanical engineering from Olin College, a SM degree in engineering systems from MIT, and a PhD degree in mechanical engineering from MIT.

Alexander H. Slocum is the Walter M. May and A. Hazel May Professor of Mechanical Engineering at MIT. He holds SB, SM, and PhD degrees in mechanical engineering from MIT, and is a member of the National Academy of Engineering.

Nomenclature

$\mathbf{A}$	Pressure matrix [Pa]
ΔP	Static pressure rise [Pa]
ΔP_L	Laminar sealing line static pressure drop [Pa]
ΔP_T	Transverse sealing line static pressure drop [Pa]
ΔP_{TL}	Long orifice static pressure drop [Pa]
ε	Surface roughness [m]
μ	Dynamic viscosity [Pa-s]
ν	Kinematic viscosity [m^2/s]
Ω	Rotational velocity [rad/s]
ρ	Fluid density [kg/m^3]
A	Fluid resistor matrix coefficient [m^3/Pa-s]
b	Sealing line width [m]
b_{long}	Longitudinal sealing line width [m]
b_{trans}	Transverse sealing line width [m]
C_p	Pressure loss coefficient [-]
C_{pL}	Laminar pressure loss coefficient [-]
C_{pT}	Turbulent pressure loss coefficient [-]
D_h	Hydraulic diameter [m]
f	Friction factor [-]
K	Laminar viscous coefficient [-]
K_L	Longitudinal laminar viscous coefficient [-]
K_T	Transverse laminar viscous coefficient [-]
L	Longitudinal cavity fluid conductivity [m^3/Pa-s]
l	Length of the rotor [m]
L^*	Dimensionless longitudinal cavity fluid conductivity [-]
l_s	Effective sealing line length [m]
P_1	First cavity relative static pressure [Pa]
P_2	Second cavity relative static pressure [Pa]
P_i	Relative static intlet pressure [Pa]

P_o Relative static outlet pressure [Pa]

P_r Nominal rotor pitch [m/rev]

P_s Nominal stator pitch [m/rev]

Q_{th} Maximum flow rate, computed from the rotor geometry [m^3/s]

R_L Longitudinal cavity sealing resistance [Pa-s/m^3]

R_r Nominal rotor radius [m]

R_s Nominal stator radius [m]

R_T Transverse cavity sealing resistance [Pa-s/m^3]

S Slip flow rate [m^3/s]

S_L Laminar slip flow rate [m^3/s]

S_T Turbulent slip flow rate [m^3/s]

T Transverse cavity fluid conductivity [m^3/Pa-s]

T^* Dimensionless transverse cavity fluid conductivity [-]

U Slip flow speed [m/s]

w Nominal clearance gap [m]

AR Area ratio [-]

E Rotor eccentricity [m]

Re Reynolds number

References

Andrade, S. F., Valério, J. V., and Carvalho, M. 2011. Asymptotic Model of the 3d Flow in a Progressing-Cavity Pump. *SPE Journal* **16** (02): 451–462.

Belcher, I. 1991. *An Investigation Into The Operating Characteristics of the Progressive Cavity Pump*. PhD thesis, Cranfield Institute of Technology.

Berton, M., Allain, O., Goulay, C., Lemetayer, P., and others 2011. Complex fluid flow and mechanical modeling of metal progressing cavity pumps PCP. In *SPE Heavy Oil Conference and Exhibition*. Society of Petroleum Engineers.

Chen, J., Liu, H., Wang, F., Shi, G., Cao, G., and Wu, H. 2013. Numerical prediction on volumetric efficiency of progressive cavity pump with fluid-solid interaction model. *Journal of Petroleum Science and Engineering* **109**: 12–17.

Edwards, M. F., Jadallah, M. S. M., and Smith, R. 1985. Head Losses in Pipe Fittings at Low Reynolds Numbers. *Chemical Engineering Research and Design* **63** (1): 43–50.

Fester, V., Kazadi, D., Mbiya, B., and Slatter, P. 2007. Loss Coefficients for Flow of Newtonian and Non-Newtonian Fluids Through Diaphragm Valves. *Chemical Engineering Research and Design* **85** (9): 1314–1324.

Gamboa, J., Olivet, A., and Espin, S. 2003. New Approach for Modeling Progressive Cavity Pumps Performance. *SPE International* **84137**.

Gamboa, J., Olivet, A., Iglesias, J., and Gonzalez, P. 2002. Understanding the performance of a progressive cavity pump with a metallic stator. In *Proceedings of the 20th International Pump Users Symposium*.

Greitzer, E. M., Tan, C. S., and Graf, M. B. 2004. *Internal Flow: Concepts and Applications*. Cambridge University Press, Cambridge.

Idelchik, I. E. and Fried, E. 1986. *Handbook of hydraulic resistance.* Washington : Hemisphere Pub. Corp., c1986.

Miller, D. S. 1978. *Internal Flow Systems*. BHRA (Information Services), Cranfield, UK, 2nd edition.

Moineau, R. 1930. *A New Capsulism*. PhD thesis, The University of Paris.

Paladino, E. E., de Lima, J. A., Pessoa, P. A., and Almeida, R. F. 2009. Computational Three Dimensional Simulation of the Flow Within Progressing Cavity Pumps. In *20th International Congress of Mechanical Engineering, Gramado, RS, Brazil*.

Pessoa, P. A., Paladino, E. E., and Lima, J. A. 2009. A simplified model for the flow in a Progressive Cavity Pump. In *20th International Congress of Mechancical Engineering COBEM, Gramado/RS, Brazil*, pages 15–20.

Vetter, G. and Wirth, W. 1995. Understanding Progressing Cavity Pumps Characteristics And Avoid Abrasive Wear. *Proceedings of the Twelfth International Pump Users Symposium* : 47–59.

Zheng, L., Wu, X., Han, G., Li, H., Zuo, Y., and Zhou, D. 2018. Analytical Model for the Flow in Progressing Cavity Pump with the Metallic Stator and Rotor in Clearance Fit. *Mathematical Problems in Engineering* **2018**: 1–14.

Zhou, X., Shi, G., Cao, G., Sun, C., He, Y., Liu, H., and Wu, H. 2013. Three dimensional dynamics simulation of progressive cavity pump with stator of even thickness. *Journal of Petroleum Science and Engineering* **106**: 71–76.